# Topological Band Transition and Corresponding Topologically Protected Interface States in Origami-based Chains

Qingqian Li

A thesis

submitted in partial fulfillment of the

requirements for the degree of

Master of Science in Aeronautics and Astronautics

University of Washington

2019

Reading Committee:

Jinkyu Yang, Chair

Marco Salviato

Program Authorized to Offer Degree:

William E. Boeing Department of Aeronautics and Astronautics

University of Washington

## Abstract

The Topological Band Transition and Corresponding Topological Protected Interface State in Two Degrees of Freedom Origami Based Chain

Qingqian Li

Chair of the Supervisory Committee:
Associate Professor Jinkyu Yang
Aeronautics and Astronautics

In this thesis, a tunable one-dimensional chain is designed based on an origami structure with two degrees of freedom. We begin this analysis by constructing the Hamiltonian matrix for the origami unit cell. This is followed by obtaining the equations-of-motion matrix for the origami finite chain using the spring-mass model. An eigenvalue analysis is conducted on the matrix obtained by both methods, which provides the dispersion curve of the origami chain. We then polarize the dispersion curve for the purpose of understanding the effects of a coupled two degrees of freedom system on the bands and bandgaps. We use the polarization to distinguish the domination of the eigenmode, i.e., translational domination, or rotational domination, for each band. We calculate the Zak phase and the sign of the impendence for each band and bandgaps so that we can study the topological inversion before and after the transition. With the determination of the band's Zak phase and the

sign of impendence of bandgaps, we discuss how the interface occurs inside the bandgaps. Based on this conceptual study, we find the topologically protected interface state in certain configurations of this highly tunable origami chain. With these results, we can use this origami chain as an exceptional energy harvesting system and transfer the rotation motion to the translational motion or the other way around.

# TABLE OF CONTENTS

# LIST OF FIGURES

# LIST OF TABLES

# ACKNOWLEDGEMENTS

I would like to thank Dr. Jinkyu Yang for giving me the opportunity to work on this project at Laboratory for Engineered Materials and Structures, University of Washington. Also, I would thank him for guiding me through this thesis. Secondly, I want to give my thanks to Dr. Marco Salviato for being my committee member and the help he gives to me. I am highly grateful for the mentoring from Dr. Hiromi Yasuda. He is a good mentor. I also want to give my thanks for the Ph.D. Candidate in My lab, Xiaotian Shi, Shuaifeng Li, and Chu-wei Chen. They are good friends and thanks for their help. Last but not least, I would thank the Department of Aeronautics and Astronautics at the University of Washington. Thanks for their time and help for the completion of this thesis.

# DEDICATION

To my beloved and supportive parents

# Chapter 1. INTRODUCTION

## 1.1 BACKGROUND AND MOTIVATIONS

Mechanical metamaterials, in recent years, have been the focal point in the engineering field and have been intensively researched [1]-[3]. They offer new perspectives and unique mechanical properties. They have abundant engineering applications, e.g., waveguide and energy harvesting [4]-[5]. origami -based structures can act as a non-conventional and special building unit for the metamaterials and show unique mechanical properties, e.g., negative Poisson's ratio and multi-stability, that attracted a lot of the attention from researchers [6]-[7]. With progressive investigation focused on the static and dynamic study of origami-based metamaterial structures, it comes naturally that people are interested in designing systems with specific vibrational properties. To design such a system, we use the correlations between the interface state and nontrivial topological invariants [9] by combining the knowledge of Topological insulators (TIs) [8]. With such properties, we can have a topologically protected interface localization in the system immune to defects. Hence, a study based on the triangulated cylindrical origami (TCO) [7] chain is initiated, and the topological phenomenon is analyzed.

## 1.2 OBJECTIVES

The goal of this thesis is using the mathematic model of TCO based one-dimensional chain to study topological band transition and its topologically protected interface state. With the topologically protected interface mode, we can design an energy harvesting system that can also transfer the rotational motion to translational motion or vice versa.

## 1.3 METHODOLOGY

In this research, the geometry, mechanical properties, and the mathematic modeling of the TCO chain are explained in chapter 2. In chapter 3, two methods are presented to construct the matrix of the TCO chain whose eigenvalues will be obtained to generate a dispersion curve. In chapter 4, we polarize the dispersion curve, determine the Zak phase of each band, and calculate the sign of the impendence of the bandgaps. Then we discuss the results of the topological transition and the interface state in the system.

# Chapter 2. BACKGROUND ON TRIANGULATED CYLINDRICAL ORIGAMI (TCO)

## 2.1 THE GEOMETRY OF TCO UNIT CELL

The geometry of the triangulated cylindrical origami (TCO) unit cell, shown in Figure 2.1. The initial height $h$ and the initial twist angle $\theta_0$ are the design parameters. With different configurations, i.e., different inputs of $h$ and $\theta_0$, the TCO unit cell will have different stiffness for folding lines $a$ and $b$ as shown in Figure 2.1. The equations governing the length of the folding lines $a$ and $b$ are shown in equation (2.1) and (2.2). The detailed calculation can be found in reference [7]. The TCO unit cell is a two degrees of freedom structure. With the force exerted on the top of the unit cell, the top surface will move along the Z- axis, and the displacement of the surface is shown as $u$ is Figure 2.1(a). Meanwhile, the top surface will also rotate with the angle of $\phi$ as shown in Figure 2.1(b).

$$a = \sqrt{(h-u)^2 + 4R^2 \sin^2(\frac{\phi}{2} + \frac{\theta_0}{2} - \frac{\pi}{2n})} \quad (2.1)$$

$$b = \sqrt{(h-u)^2 + 4R^2 \sin^2(\frac{\phi}{2} + \frac{\theta_0}{2} + \frac{\pi}{2n})} \quad (2.2)$$

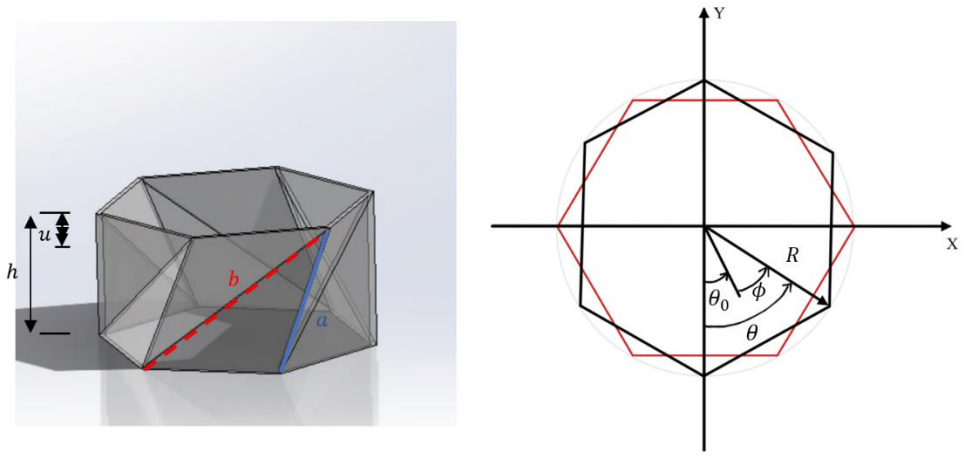


$(a)$ $(b)$

Figure 2.1. Graph (a) is the 3D Geometry of the TCO unit cell with the polygon side number of 6. h is the height. u is the displacement in Z-direction when the force exerted on the top. a and b are the folding line and the corresponding crease line shown in the folding pattern in Figure 1.2. Graph (b) is the top view of the very same TCO unit cell. The red lines indicate hexagon is at the bottom, and the black lines indicate the top. $\theta_0$ is the initial twist angle. $\phi$ is the rotation angle when the unit cell is pushed. $\theta$ is the total ration angle.

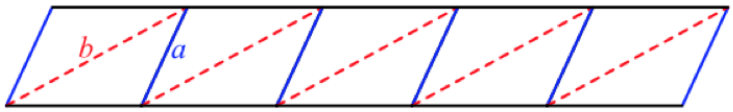


Figure 2.2. The folding pattern of the TCO unit cell. Folding line a, solid blue line, folds outward, mountain-like. Folding line b, red dash line, is fold inward, valley-like.

## 2.2 THE KINEMATICS OF THE TCO UNIT CELL

The two degrees of freedom mathematical model of the TCO structure can be derived with the method of conservation of energy. We can analyze the kinematics of the TCO unit cell based on this mathematical model. Equation (2.4) is the equation of elastic potential energy. The detailed calculation can be found in reference [10]. The model utilizes linear springs to simulate the folding motion of the unit, e.g., length change of the folding lines a and b with spring stiffnesses of $k_a \; and \; k_b$ respectively.

$$U(u,\phi) = \frac{1}{2}nk_a(a-a_0)^2 + \frac{1}{2}nk_b(b-b_0)^2 \tag{2.4}$$

$a_0$ and $b_0$ are the initial lengths before the folding motion. The values of a and b can be found in equation (2.1) and (2.2). *n* is the number of the sides the polygon has for the configuration.

Using the principle of minimum potential energy, the force-displacement relation, and the torque-rotation relation of the system can be found by taking the derivatives of the potential energy equation shown in (2.4). The detailed derivation is shown in reference [11].

$$F(u,\phi) = \frac{\partial U}{\partial u}$$
$$= nk_aR^2(h-u)\left(1-\frac{a_0}{a}\right) + nk_bR^2(h-u)\left(1-\frac{b_0}{b}\right) \tag{2.5}$$
$$T(u,\phi) = \frac{\partial U}{\partial \phi}$$
$$= nk_aR^2\left(1-\frac{a_0}{a}\right)\sin\left(\phi+\theta_0-\frac{\pi}{n}\right) + nk_bR^2\left(1-\frac{b_0}{b}\right)\sin\left(\phi+\theta_0-\frac{\pi}{n}\right) \tag{2.6}$$

## 2.3 EQUATIONS OF THE MOTION OF THE TCO CHAIN

In this section, we will discuss the configuration of the TCO based chain and its equations of motion. The TCO formed chain is shown in Figure 2.3. As shown, the TCO chain will connect along the Z-direction, and there will be plates assembled on the top and bottom of the surfaces. For the chain configuration, there will be two types. The monomer chain, form with the same TCO unit cell; and the dimer chain, form with two different configurations of the TCO unit cell. As introduced in the last section, the configurations of the TCO unit cell depend on the initial height and initial twist angle. For the convenience of the analysis, by only changing the initial twist angle,

we can have a different TCO unit cell to form the dimer chain. By changing the initial twist angle, the stiffness constant for the folding line a and b will change. This change will affect the equations of motion of the chain as well as the matrix used to obtain the dispersion curve, i.e., band structure, of the chain. From the mathematical model of the TCO unit cell and treating the chain as a spring-mass system, shown in Figure 2.4, we can model the equations of motion for the system as shown in the equations (2.7) and (2.8) [11].

$$M_j\ddot{u}_j = F\left(u_{j-1} - u_j, \phi_{j-1} - \phi_j\right) - F(u_j - u_{j+1}, \phi_j - \phi_{j+1}) \tag{2.7}$$

$$J_j\ddot{\phi}_j = T\left(u_{j-1} - u_j, \phi_{j-1} - \phi_j\right) - T(u_j - u_{j+1}, \phi_j - \phi_{j+1}) \tag{2.8}$$

In these equations, *j* is the index number of the TCO unit. *F* is the force, and *T* is the torque. *M* is the mass of the plate located at the top and bottom surface. *J* is the moment of inertia of the plate mount on the two ends of the unit cell.

The force-displacement and torque-rotation equations of the TCO unit cell are highly non-linear. We linearized these equations (2.5), (2.6) using Taylor expansion by assuming small displacement and rotation, at $u = 0\ and\ \phi = 0$. The equations after the linearization are shown as follows.

$$F = \alpha_{uu}u + \alpha_{u\phi}\phi \tag{2.9}$$

$$T = \alpha_{u\phi}u + \alpha_{\phi\phi}\phi \tag{2.10}$$

Where $\alpha_{uu}, \alpha_{u\phi}\ and\ \alpha_{\phi\phi}$ [11] are the constants after the linearization, $\alpha_{uu} = \frac{\partial F}{\partial u}(0), \alpha_{u\phi} = \frac{\partial F}{\partial \phi}(0) = \frac{\partial T}{\partial u}(0), \alpha_{\phi\phi} = \frac{\partial T}{\partial \phi}(0),$ and their expressions are:

$$\alpha_{uu} = nh^2\left(\frac{k_a}{a_0^2} + \frac{k_b}{b_0^2}\right) \tag{2.11}$$

$$\alpha_{u\phi} = -\frac{nk_aR^2hsin\left(\theta_0-\frac{\pi}{n}\right)}{a_0^2} - \frac{nk_bR^2hsin\left(\theta_0+\frac{\pi}{n}\right)}{b_0^2} \quad (2.12)$$

$$\alpha_{\phi\phi} = \frac{nk_aR^4\sin^2\left(\theta_0-\frac{\pi}{n}\right)}{a_0^2} + \frac{nk_bR^4\sin^2\left(\theta_0+\frac{\pi}{n}\right)}{b_0^2} \quad (2.13)$$

The $k_a$ and $k_b$ is the stiffness of the folding lines, and the superposition of all the folding lines should account toward the calculations.

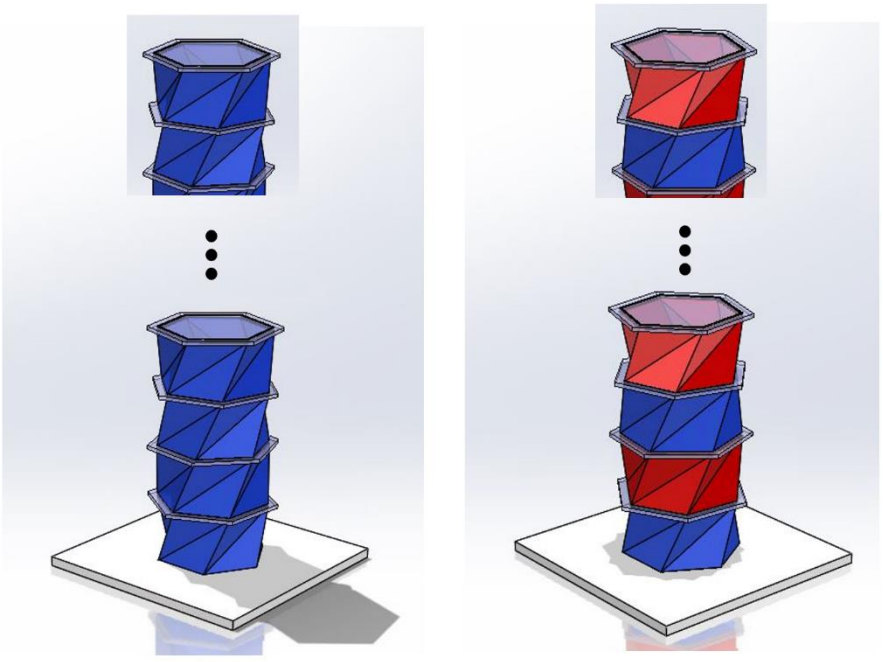

(a) (b)

Figure 2.3. In graph (a), it is showing the TCO formed monomer chain. All the TCO unit will have the same initial height and same initial twist angle. In graph (b), it is showing a dimer chain, and the blue type TCO unit cell and the red unit cell will have the same initial height but different initial twist angle. Here we name the dimer chain unit cell with blue color as (1) and red as (2).

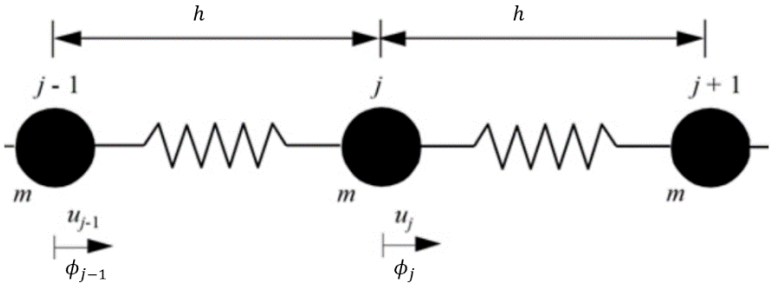


Figure 2.4. Spring-mass model used as the mathematic model for analysis TCO chain. *j* is the index of the unit.

# Chapter 3. EIGENVALUE ANALYSIS ON UNIT CELL AND FINITE CHAIN OF THE TCO CHAIN.

## 3.1 UNIT CELL ANALYSIS OF THE TCO CHAIN

In section 2.3, we have the equations of motion for the system of the TCO chain. We now can build the Hamiltonian matrix for the system. Plugging in the linearized force equation and torque equation, (2.9), (2.10), into the equations of motion (2.7), (2.8), yields the linearized equations of motion for the TCO chain shown in (3.1) -(3.4).

$$M_j \ddot{u}_j^{(1)} =$$

$$-\alpha_{uu}^{(1)}\left(u_j^{(1)} - u_{j-1}^{(2)}\right) + \alpha_{uu}^{(2)}\left(u_j^{(2)} - u_j^{(1)}\right) - \alpha_{u\phi}^{(1)}\left(\phi_j^{(1)} - \phi_{j-1}^{(2)}\right) + \alpha_{u\phi}^{(2)}\left(\phi_j^{(2)} - \phi_j^{(1)}\right) \quad (3.1)$$

$$J_j \ddot{\phi}_j^{(1)} =$$

$$-\alpha_{u\phi}^{(1)}\left(u_j^{(1)} - u_{j-1}^{(2)}\right) + \alpha_{u\phi}^{(2)}\left(u_j^{(2)} - u_j^{(1)}\right) - \alpha_{uu}^{(1)}\left(\phi_j^{(1)} - \phi_{j-1}^{(2)}\right) + \alpha_{uu}^{(2)}\left(\phi_j^{(2)} - \phi_j^{(1)}\right) \quad (3.2)$$

$$M_j \ddot{u}_j^{(2)} =$$

$$\left(u_{j+1}^{(1)} - u_j^{(2)}\right) - \alpha_{uu}^{(2)}\left(u_j^{(2)} - u_j^{(1)}\right) + \alpha_{u\phi}^{(1)}\left(\phi_{j+1}^{(1)} - \phi_j^{(2)}\right) - \alpha_{u\phi}^{(2)}\left(\phi_j^{(2)} - \phi_j^{(1)}\right) \quad (3.3)$$

$$J_j \ddot{\phi}_j^{(2)} =$$

$$\alpha_{u\phi}^{(1)}\left(u_{j+1}^{(1)} - u_j^{(2)}\right) - \alpha_{u\phi}^{(2)}\left(u_j^{(2)} - u_j^{(1)}\right) + \alpha_{uu}^{(1)}\left(\phi_{j+1}^{(1)} - \phi_j^{(2)}\right) - \alpha_{uu}^{(2)}\left(\phi_j^{(2)} - \phi_j^{(1)}\right) \quad (3.4)$$

The superscripts (1) and (2) are two different types of the TCO unit cell in the chain. When all the TCO unit cells are the same configuration such as in the case of the monomer chain, the constants with different superscripts are the same. *j* is the index of the TCO unit cell in the chain. It represents the location of the unit cell.

Now we can plug in the solution for the wave equation, (3.5), (3.6), in the systems of equations (3.1) -(3.4). k in the following equation is the wave number, and i is the imaginary number.

$$u_j^{(1)} = u^{(1)} e^{i(2kjh-\omega t)}\,;\; u_j^{(2)} = u^{(2)} e^{i(2kjh-\omega t)} \tag{3.5}$$

$$\phi_j^{(1)} = \phi^{(1)} e^{i(2kjh-\omega t)}\,;\; \phi_j^{(2)} = \phi^{(2)} e^{i(2kjh-\omega t)} \tag{3.6}$$

Therefore, the Hamiltonian matrix for this mechanical system can be found [11].

$$-\omega^2 \begin{bmatrix} u^{(1)} \\ \phi^{(1)} \\ u^{(2)} \\ \phi^{(2)} \end{bmatrix} = \begin{bmatrix} -\frac{\alpha_{uu}^{(1)}+\alpha_{uu}^{(2)}}{M_j} & -\frac{\alpha_{u\phi}^{(1)}+\alpha_{u\phi}^{(2)}}{M_j} & \frac{\alpha_{uu}^{(1)}+\alpha_{uu}^{(2)}e^{-2ikh}}{M_j} & \frac{\alpha_{u\phi}^{(1)}+\alpha_{u\phi}^{(2)}e^{-2ikh}}{M_j} \\ -\frac{\alpha_{u\phi}^{(1)}+\alpha_{u\phi}^{(2)}}{J_j} & -\frac{\alpha_{\phi\phi}^{(1)}+\alpha_{\phi\phi}^{(2)}}{J_j} & \frac{\alpha_{u\phi}^{(1)}+\alpha_{u\phi}^{(2)}e^{-2ikh}}{J_j} & \frac{\alpha_{\phi\phi}^{(1)}+\alpha_{\phi\phi}^{(2)}e^{-2ikh}}{J_j} \\ \frac{\alpha_{uu}^{(1)}+\alpha_{uu}^{(2)}e^{2ikh}}{M_j} & \frac{\alpha_{u\phi}^{(1)}+\alpha_{u\phi}^{(2)}e^{2ikh}}{M_j} & -\frac{\alpha_{uu}^{(1)}+\alpha_{uu}^{(2)}}{M_j} & -\frac{\alpha_{u\phi}^{(1)}+\alpha_{u\phi}^{(2)}}{M_j} \\ \frac{\alpha_{u\phi}^{(1)}+\alpha_{u\phi}^{(2)}e^{2ikh}}{J_j} & \frac{\alpha_{\phi\phi}^{(1)}+\alpha_{\phi\phi}^{(2)}e^{2ikh}}{J_j} & -\frac{\alpha_{u\phi}^{(1)}+\alpha_{u\phi}^{(2)}}{J_j} & -\frac{\alpha_{\phi\phi}^{(1)}+\alpha_{\phi\phi}^{(2)}}{J_j} \end{bmatrix} \begin{bmatrix} u^{(1)} \\ \phi^{(1)} \\ u^{(2)} \\ \phi^{(2)} \end{bmatrix} \tag{3.7}$$

Solve the eigenvalue problems, $\det(\mathbf{\Lambda} - \boldsymbol{\lambda}\mathbf{I}) = 0$, for $\omega$ at each wave number, k. And the frequency of the system would be $f = \frac{\omega}{2\pi}$,

## 3.2 FINITE CHAIN ANALYSIS OF THE TCO CHAIN

Different than the unit cell analysis, in this part, we plug in $u_n = u_{0,n}e^{i\omega t}$ $and$ $\phi_n = \phi_{0,n}e^{i\omega t}$ to equations of motion. Hence a discretized eigenvalue is yield as shown in equation(3.8) and solve the eigenvalue problem $\det(\mathbf{\Lambda} - \boldsymbol{\lambda}\mathbf{I}) = 0$ for $\lambda$. where $\mathbf{\Lambda} = \mathbf{M^{-1}}\boldsymbol{B}$, $\lambda = -\omega^2$, and B is the stiffness matrix of the system. The frequency, f, of the system would be $f = \frac{\omega}{2\pi}$.

$$\lambda \boldsymbol{u} = \mathbf{\Lambda} \boldsymbol{u} \tag{3.8}$$

Now we can construct the mass matrix of the TCO chain, as shown in (3.9). It is a diagonal matrix. The stiffness matrix of the system can be constructed as shown in (3.10) where the size of the matrix is *m* by *m*, and *m* is the total number of TCO unit cells in the chain.

$$\mathbf{M} = \begin{bmatrix} M_1 & 0 & \cdots & 0 & 0 & \cdots & 0 & 0 \\ 0 & J_1 & \cdots & 0 & 0 & \cdots & 0 & 0 \\ \vdots & \vdots & \ddots & \cdots & \cdots & \ddots & \vdots & \vdots \\ 0 & 0 & \cdots & M_j & 0 & \ddots & \ddots & 0 \\ 0 & 0 & \cdots & 0 & J_j & \ddots & \ddots & 0 \\ \vdots & \vdots & \ddots & \ddots & \ddots & \ddots & \ddots & \vdots \\ \vdots & \vdots & \ddots & 0 & 0 & \ddots & M_n & 0 \\ 0 & 0 & \cdots & 0 & 0 & \cdots & 0 & J_n \end{bmatrix} \tag{3.9}$$

$$\boldsymbol{B} =$$

$$\begin{bmatrix} -(\alpha_{uu}^{(1)} + \alpha_{uu}^{(2)}) & -(\alpha_{u\phi}^{(1)} + \alpha_{u\phi}^{(2)}) & \alpha_{uu}^{(2)} & \alpha_{u\phi}^{(2)} & 0 & 0 & 0 \\ -(\alpha_{u\phi}^{(1)} + \alpha_{u\phi}^{(2)}) & -(\alpha_{\phi\phi}^{(1)} + \alpha_{\phi\phi}^{(2)}) & \alpha_{u\phi}^{(2)} & \alpha_{\phi\phi}^{(2)} & 0 & 0 & \cdots \\ \alpha_{uu}^{(2)} & \alpha_{uu}^{(2)} & -(\alpha_{uu}^{(1)} + \alpha_{uu}^{(2)}) & -(\alpha_{u\phi}^{(1)} + \alpha_{u\phi}^{(2)}) & \alpha_{uu}^{(1)} & \alpha_{u\phi}^{(1)} & \vdots \\ \alpha_{u\phi}^{(2)} & \alpha_{\phi\phi}^{(2)} & -(\alpha_{u\phi}^{(1)} + \alpha_{u\phi}^{(2)}) & -(\alpha_{\phi\phi}^{(1)} + \alpha_{\phi\phi}^{(2)}) & \alpha_{u\phi}^{(1)} & \alpha_{\phi\phi}^{(1)} & \ddots \\ 0 & 0 & \alpha_{uu}^{(1)} & \alpha_{u\phi}^{(1)} & \ddots & \ddots & \ddots \\ 0 & 0 & \alpha_{u\phi}^{(1)} & \alpha_{\phi\phi}^{(1)} & \ddots & \ddots & \ddots \\ \vdots & \vdots & \cdots & \cdots & \ddots & \cdots & \cdots \end{bmatrix} \quad (3.10)$$

Different than the unit cell analysis, the frequency calculated by using this method is matched with the unit number of the chain, m. We use the Fast Fourier Transform to rearrange the frequency to match the wave number to obtain the dispersion curve.

# Chapter 4. DISPERSION CURVE AND INTERFACE MODE OF TCO CHAIN.

## 4.1 DISPERSION CURVE OF THE TCO CHAIN.

In the last section, we constructed the Hamiltonian matrix, as well as the matrix based on the finite chain method for the TCO chain system. Now by doing eigenvalue analysis, we can plot the dispersion curve for the two TCO chain configurations: monomer chain and dimer chain. In this section, we will first discuss the unique properties of the dispersion curves of the TCO chains. For the one-degree-of-freedom spring-mass system, the dispersion curves only have one pair of modes. The lower one is called the acoustic band, and the upper one is called the optical band. For the two-degrees-of-freedom TCO chain, the dispersion curve, as shown in Figure 4.1., will have two pairs of mode.

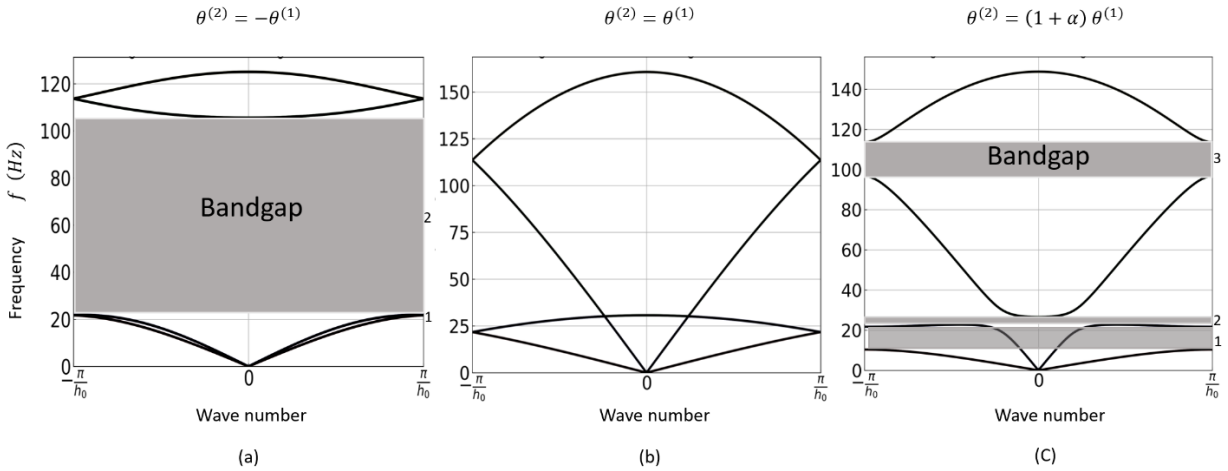


Figure 4.1. Graph (a) showing dispersion curve of dimer TCO chain with the chain configuration as (1)-(2)-(1)-(2), with the unit (1) have $\theta_0^{(1)} = 60°$ and unit (2) with $\theta_0^{(2)} = -60°$. The gray area is bandgap, and the numbering of the bandgaps are showing on the right. Graph (b) showing the dispersion curve of monomer chain with all unit cell's initial twist angle of $\theta_0^{(1)} = \theta_0^{(2)} = 60°$. Graph (c) showing the dispersion curve with the dimer chain configuration setup with the unit (1) have $\theta_0^{(1)} = 60°$ and unit (2) with $\theta_0^{(2)} = (1+\alpha)60°$. The gray area is bandgap, and the numbering of the bandgaps are showing on the right.

TCO unit cell is highly tunable; there are many ways to change the stiffness. So, we specifically selected two ways to construct the dimer chain. First, we select the initial twist angle for one-unit cell, $\theta_0^{(1)}$, and for the second unit cell, we select the initial twist angle as $\theta_0^{(2)} = -\theta_0^{(1)}$. The second way is to set the second twist initial angle as a function of the first initial twist angle as $\theta_0^{(2)} = (1+\alpha)\theta_0^{(1)}$, where $\alpha$ is a constant to vary, and by changing this constant, we can have multiple initial twist angles for the second unit cell. For this case, we select $\alpha = 0.5$.

As shown in Figure 4.1 (a), by choosing the unit cell (2) to have negative direction but the same angle in magnitude we can open only the crossing point that is not on the boundary of Brillouin zone [15]. The stiffness constant for this case would be $\alpha_{uu}^{(1)} = \alpha_{uu}^{(2)}, \alpha_{\phi\phi}^{(1)} = \alpha_{\phi\phi}^{(2)}, \alpha_{u\phi}^{(1)} = -\alpha_{u\phi}^{(2)}$. As another unique point about the two degrees of freedom system, in the equations of motion, we have a coupled term in both force and torque equations. And as shown in this case, by changing the values of the coupled term, we can open the intersection point between the second and third band.

For the case of the monomer chain, Figure 4.1 (b), the twist angle of the TCO unit cells will have the same initial twist angle and will have the same stiffness constants, $\alpha_{uu}^{(1)} = \alpha_{uu}^{(2)}, \alpha_{\phi\phi}^{(1)} = \alpha_{\phi\phi}^{(2)}, \alpha_{u\phi}^{(1)} = \alpha_{u\phi}^{(2)}$. At the boundary of the Brillouin zone, there will be two high folding points. Also, in the TCO system, there will be a crossing point between the higher acoustic band and the lower optical band. By changing the stiffness constant and the initial twist angle, we can open these three points.

In Figure 4.1 (c), The dimer chain is constructed by choosing the second unit cell initial twist angle as the function of the initial twist angle of the first unit cell and in this case $\alpha = 0.5$. The

stiffnesses will be: $\alpha_{uu}^{(1)} > \alpha_{uu}^{(2)}, \alpha_{\phi\phi}^{(1)} > \alpha_{\phi\phi}^{(2)}, \alpha_{u\phi}^{(1)} < \alpha_{u\phi}^{(2)}$. At this configuration, all the stiffness constants are different for the both unit cells. The different stiffness constants will open the high folding point at the boundary of the Brillouin zone. Also, with the different coupled term, the intersection point will also open just the same as the case shown in (a).

## 4.2 POLARIZATION OF THE DISPERSION CURVE.

In this section, we polarize the eigenmode and plot on the same graph as the dispersion curve. The normalization of the eigenvectors of the system are calculated following equation (4.1). The first eigenmode is selected as the baseline. The first eigenmode can represent the relation of the rotational motion and the translational motion after the linearization of the force-displacement motion and the torque-rotation motion. Details can be found in Figure 2(c) in reference [10]. Based on the value of P calculated in equation (4.1), the magnitude of the translational motion dominates when P is 1, and vice versa. The polarized graphs are shown in Figure 4.2. The color of each point represents the value of P. The red dots means that at the frequency, the mode shape is translational dominated in magnitude. Blue means the mode shape is rotational dominated in magnitude. Lastly, yellow means the translational motion and rotational motion mix and the mode shape cannot be distinguished. The results show when the twist angle of the second unit cell is in the opposite direction with the same magnitude, $\theta_0^{(2)} = -\theta_0^{(1)}$, the mode shape can be clearly distinguished but for the other two cases, the eigenmode shape mix between the translational motion and the rotational cannot be clearly identified. Observe the graph (a) in Figure 4.2. There is a domination transition between the translational motion and rotational motion at the 2nd and 3rd band. In order to separating the translational dominant mode and rotational dominant mode, the polarization of

the TCO chain is not successful based on the observation described above These configurations all show a mixed mode shape.

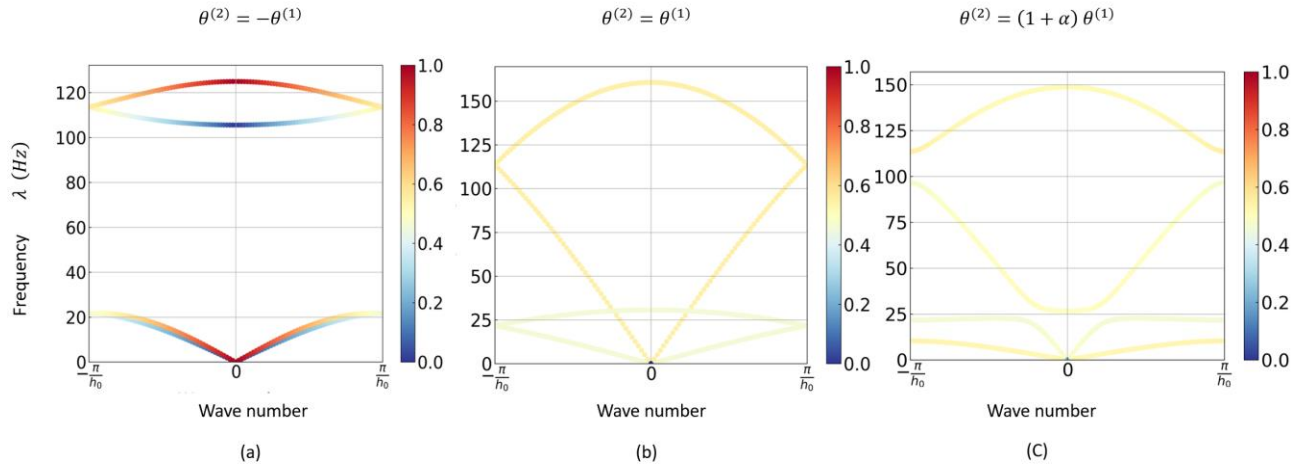


Figure 4.2. Graph (a), (b) and (c) have the same set up as Figure 4.1 and with the polarization value P superimposed in the figure. The red color means the translational motion dominates in magnitude, and the blue color means the rotational motion dominates in magnitude. The yellow means the mode's polarization very close to each other, and no domination in magnitude can be clearly identified.

$$P = \frac{u^{(1)}+u^{(2)}}{u^{(1)}+\phi^{(1)}\frac{u^{(1)}_{1st}}{\phi^{(1)}_{1st}}+u^{(2)}+\phi^{(2)}\frac{u^{(2)}_{1st}}{\phi^{(2)}_{1st}}} \tag{4.1}$$

## 4.3 ZAK PHASE OF THE BAND AND THE IMPEDANCES OF THE BAND GAP IN TCO CHAIN SYSTEM.

In the purpose of finding the band transition to study the topologically protected interface state of the TCO chain system, the Zak phase of each band was calculated with the three cases as shown in section 4.1 and 4.2. We can find the symmetry of each band and identify the band inversion [9] pass the transition point with the value of the Zak phase of each band. As shown in Figure 4.3, the Zak phase of each band was calculated. For the case with the unit (1) having $\theta_0^{(1)} = 60°$ and unit (2) with $\theta_0^{(2)} = -60°$, the band structure including a degenerate point. In this situation, the zero point is excluded and the initial twist angle for unit 2 is approximated to avoid the degenerate point on the edge of the Brillouin zone when calculate the Zak phase of the lower two bands.

The equation for calculating the Zak phase of the band is shown in the equation (4.2) [13]-[16]. The equation for calculating the sign of the impendence of the band gap is shown in (4.3) [13]. In this equation, n is the number of the bandgap starting from 1, m is the number of the band starting from 0, and l is the intersection point under the band gap. If the calculated sign of impendence for the bandgaps is different before and after the transition, then the band gap has an interface state; otherwise, an interface state does not exist.

$$\theta_n^{Zak} = i \int_{-\frac{\pi}{h}}^{\frac{\pi}{h}} < u_k | \partial_k u_k > dk \tag{4.2}$$

$$Sgn[\zeta^n] = (-1)^n (-1)^l \exp(i \sum_{m=0}^{n-1} \theta_m^{Zak}) \tag{4.3}$$

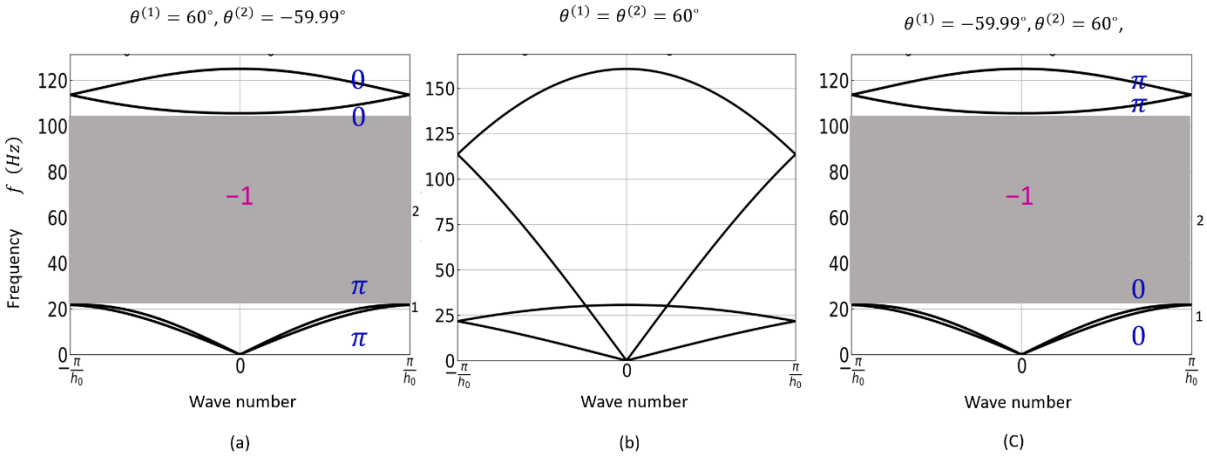


Figure 4.3. Graph (a) show the configuration of (1)-(2)-(1)-(2) with the initial twist angle of $\theta_0^{(1)} = 60°$ and $\theta_0^{(2)} = -60°$degrees (b) is the transition point with the unit (1) and (2) have the same initial twist angle, $\theta_0^{(1)} = \theta_0^{(2)} = 60°$. And (c) is showing the configuration of (1)-(2)-(1)-(2) with the initial twist angle of $\theta_0^{(1)} = -60°$and $\theta_0^{(2)} = 60°$ degrees. The order of the unit cell is switched. The Zak phase of each band for both before the transition and after the transition is shown in the graph (a) and (c). The Zak phase value mark, as bule color, beside the bands. The sign of impendence is shown inside the bandgaps, marked as magenta.

In Figure 4.3 and 4.4, The dispersion curve of two different configurations of the TCO chain is shown. And in both cases, we switch the unit cell order and calculate their Zak phase in order to check their band symmetries. If these two setups in each configuration have band inversion and have a common band gap, it will create a topological defect when they are connected and this will lead to the creation of the topologically protected interface state.

As shown in Figure 4.3, we observe the second and third band have a band inversion by passing the transition configuration. The Zak phase for the 2nd band and 3rd band of the first chain configuration is $\pi \; and \; 0$. After the transition configuration, the 2nd band and 3rd band of the second chain configuration is $0 \; and \; \pi$. The Zak phase of each band in this configuration was calculated using equation (4.3). With the Zak phase of each band, we can find the sign of the impendence of the bandgaps. For initial twist angle of the first cell and second cell of 60 and -60 degrees, the sign of the band gap is -1. For the initial twist angle of the first cell and second cell of -60 and 60 degrees, the sign of the band gap is also -1. The calculation is based on the equation (4.3). For both configurations, the bandgap number n is 2 and there is no intersection point below this bandgap. There is a band inversion between the second and third band, however, the impendence is the same. Hence there will not be an interface state with the same sign of the impendence.

The second configuration is shown in Figure 4.4. In this configuration, three bandgaps are shown in the dispersion curve. The first bandgap is between band 1 and 2, the second bandgap is between the second and third bands, and the last band gap is between the third band and fourth band. Note that the first bandgap is not a complete bandgap.

As shown in Figure 4.4, we observe that all the bands have a band inversion by passing the transition configuration. The Zak phase for the 1st band and 2nd band of the first chain configuration is $0 \; and \; \pi$. After the transition configuration, the 1st band and 2nd band of the second chain

configuration is $\pi \; and \; 0$. The Zak phase for the 2nd band and 3rd band of the first chain configuration is $\pi \; and \; \pi$. After the transition configuration, the 2nd band and 3rd band of the second chain configuration is $0 \; and \; 0$. The Zak phase for the 3rd band and 4th band of the first chain configuration is $\pi \; and \; 0$. After the transition configuration, the 3rd band and 4th band of the second chain configuration is $0 \; and \; \pi$

We can calculate the sign of impendence of each bandgap, with the Zak phase calculated for each band. The first bandgap for setup shown in Figure 4.4 (a) is -1, for setup shown in Figure 4.4 (b) is 1. And there is a band inversion. Hence for the first bandgap, the interface is topologically protected. For the second bandgap, there is a band inversion between the 2nd and 3rd band. The impendence is -1 for both Figure 4.4 (a) and (b). So there will not be an interface state with the same sign of the impendence. For the third Bandgap, the 3rd and 4th band have band inversion. The impendence of the bandgap is -1 for (a) and 1 for (b). Hence the interface is topologically protected.

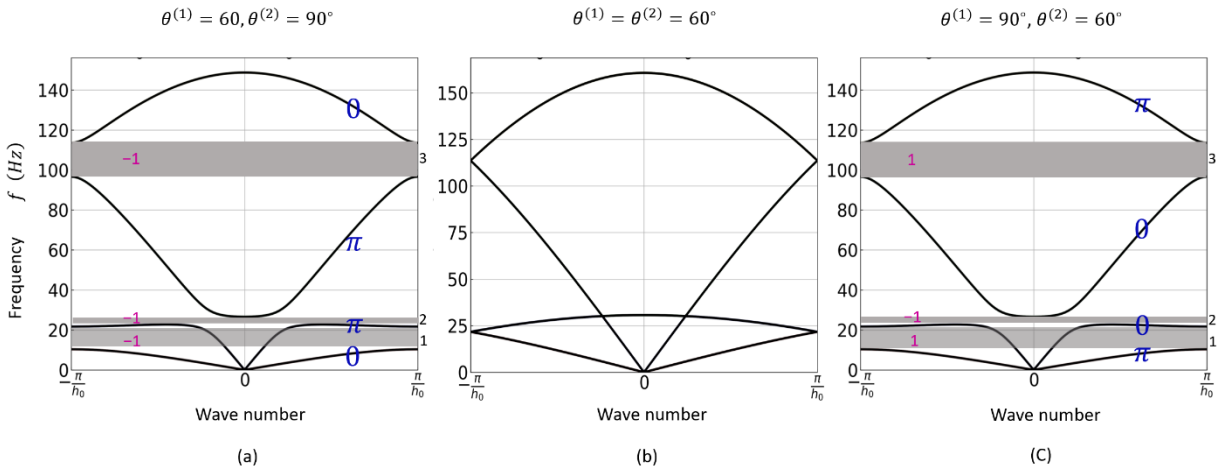


Figure 4.4. Graph (a) show the configuration of (1)-(2)-(1)-(2) with the initial twist angle of 60 and 90 degrees and (c) is showing the configuration with (1)-(2)-(1)-(2) with the initial twist angle of 90 and 60 degrees. The order of the unit cell is switched. Graph (b) is the transition point with the same initial twist angle. The Zak phase of each band has shown in the part (a) and (c). The Zak phase value mark beside the bands, as bule color. The sign of impendence is shown inside the bandgaps, marked as magenta.

## 4.4 THE INTERFACE STATE.

In the last section, we analyze the Zak phase and the impendence of the bandgap for two different configurations. In this section, we will use a finite chain to plot the interface state. The chain configuration is the same as the last section. There will be two different dimer configurations for the TCO chain. However, the difference in this section is we connected the configuration before the transition and after. The interface states and finite chain results are shown in Figure 4.5. In graph (a) the chain contains a total of 160 units. Units 1 to 80 have the configuration with $\theta_0^{(1)} = 60°$ and $\theta_0^{(2)} = -60°$ and the rest have the configuration of $\theta_0^{(1)} = -60°$ and $\theta_0^{(2)} = 60°$. The interface state and the dispersion curve based on the finite chain analysis are shown in the Figure. In Figure 4.5 (b), the interface states and finite chain results are shown, for the configuration the chain contains a total of 160 units. Units 1 to 80 have the configuration with $\theta_0^{(1)} = 60°$ and $\theta_0^{(2)} = 90°$ and the rest have the configuration of $\theta_0^{(1)} = 90°$ and $\theta_0^{(2)} = 60°$.

By observing the mode shape of those states shown in the bandgaps, we can find the interface state. For the interface mode, the mode shape will have a localization at the interface where the two chains are connected. Also, there will be edge states too. They only have localization on the edges of the chain. We will not focus on the edge state but only the interface state.

For the unit cell analysis, the boundary condition of the chain is fixed on one end and free on the other. As shown in Figure 4.5 (a), there are three eigenmodes that stand out in the bandgap, and two of the states have the same frequency at 80Hz. These two are the edge states. One of the eigenmodes is showing a very distinctive edge state mode shape. The other state's mode shape is very similar to an interface mode. However, it has the same frequency as the edge state. Hence it is the combined edge state with two connected TCO chains. The mode shape located at 25 Hz is an interface state. However, it is contradictory with the result of the calculation on the sign of impendence. The occurrence of this interface mode may not be related to the band inversion. From the study on the polarization of these types of the configuration, the intersection point of the second and third band will affect the eigenmode on these two bands. There is interchange on the eigenmode even after the opening of the intersection point.

For Figure 4.5 (b), the results are consistent with the Zak phase calculation and sign of the impendence. We found two eigenmodes with the frequency inside the third bandgap, and one of them is an edge mode by observing the mode shape of the state, the localization is at the edge of

the chain. And the other is the topologically protected interface mode with the localization at the center where the chain is connected. In the first bandgap, we find an interface mode and it is topologically protected. The mode shape of the state is localized at the interface.

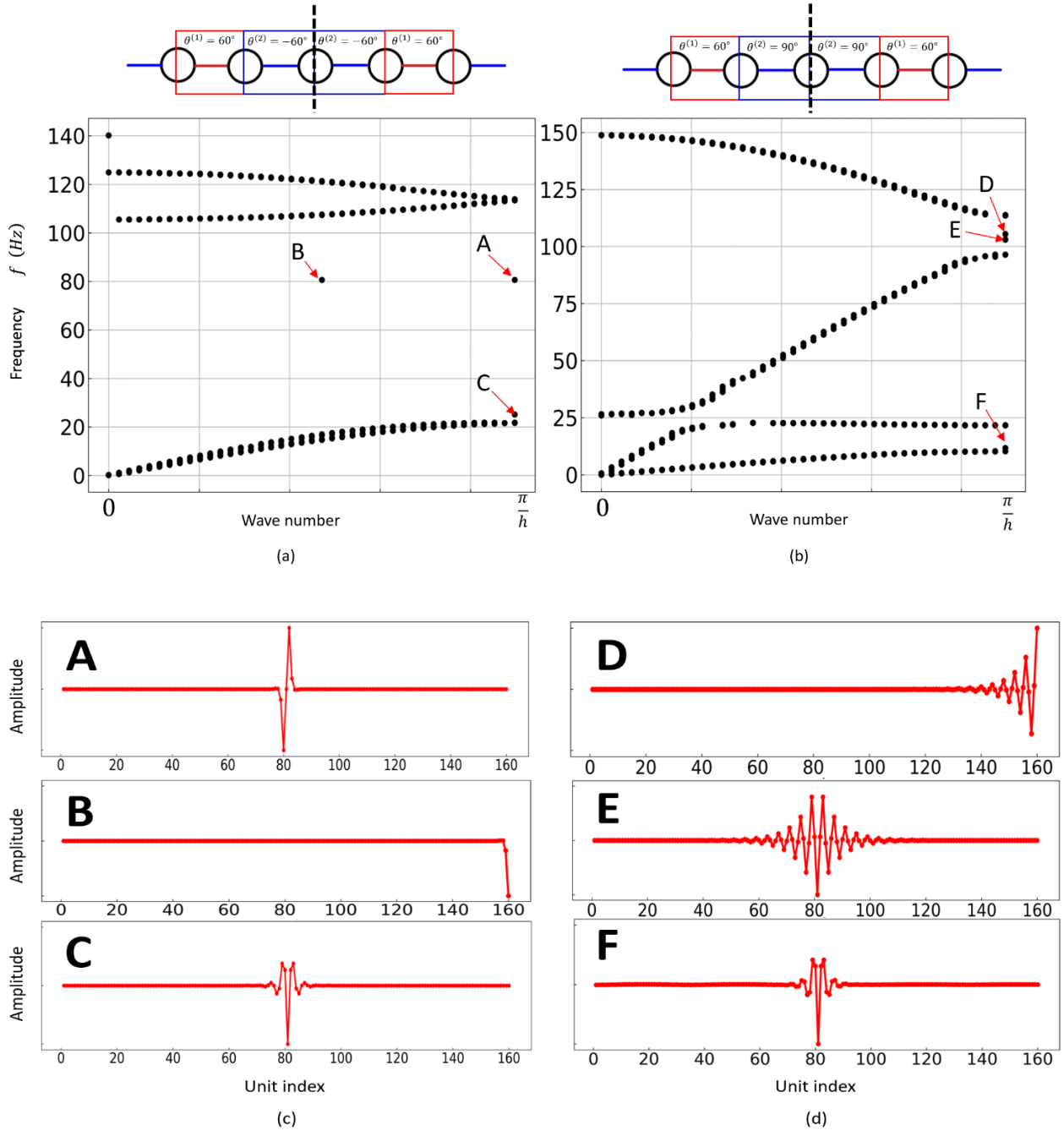


Figure 4.5. Graph (a) shows the dispersion curve solved with finite chain analysis of the configuration with a total of 160 units. Units 1 to 80 have the configuration with $\theta_0^{(1)} = 60°$ and

$\theta_0^{(2)} = -60°$ and the rest have the configuration of $\theta_0^{(1)} = -60°$ and $\theta_0^{(2)} = 60°$. The figure above (a) showing the configuration of connected chain. The dash line is the interface. There are three eigenmodes located in the bandgap. Their mode shape is shown in the graph (c), and the letters are corresponding to the mode marked in graph (a). In Graph (b), a configuration of the chain contains a total of 160 units. Units 1 to 80 have the configuration with $\theta_0^{(1)} = 60°$ and $\theta_0^{(2)} = 90°$ and the rest have the configuration of $\theta_0^{(1)} = 90°$ and $\theta_0^{(2)} = 60°$. The figure above (b) showing the configuration of connected chain. The dash line is the interface. There are three eigenmode located in the bandgap. Their mode shape is shown in the graph (d), and the letters are corresponding to the mode marked in graph (b).

# Chapter 5. CONCLUSION AND FUTURE WORK.

In conclusion, we use the mathematical model for the TCO unit cell to successfully calculate the dispersion curve of the system. There are two different methods used: unit cell analysis and finite chain method. We study two configurations of the TCO chain, monomer chain and dime chain. For the dimer chain, we select two different ways to build up the TCO dimer chain and analyze the corresponding band structure and then we calculate the Zak phase and sign of impendence for the bandgaps. For the two configurations we selected, there are two topologically protected interface modes that exist in the chain with $\theta_0^{(1)} = 60°$ and $\theta_0^{(2)} = 90°$ connected with a chain of twist angles of $\theta_0^{(1)} = 90°$ and $\theta_0^{(2)} = 60°$. One of the topologically protected interface states is at the complete bandgap and can be used as the design for energy harvesting system and can also used to transfer the rotational motion to the translational motion.

However, there is an interface state that also occurs in the bandgap for the configuration of chain with $\theta_0^{(1)} = 60°$ and $\theta_0^{(2)} = -60°$ connected with the chain of twist angles of $\theta_0^{(1)} = -60°$ and $\theta_0^{(2)} = 60°$. It is not agreed with the calculation of the Zak phase and the sign of impendence. Based on the calculation, there will be no interface state at the bandgap. So, the localization is not topologically protected. And based on the reference [16]-[18], the mode interchange is very common in the multi degrees of freedom system. And curve veering is also related to the localization of the system. This would be the future exploration to explain the localization in the second bandgap. From the topological perspective, there are very few papers discussing the intersection point that is not at the boundary of Brillouin zone. A mathematical way to analysis this behavior needs to be considered.

# BIBLIOGRAPHY


[1] M. Wegener, *Metamaterials Beyond Optics*, Science, 2013.

[2] C. Coulais, D. Sounas, A. Alu, *Static non-reciprocity in mechanical metamaterials*, Nature, 2017.

[3] G. Ma, P. Sheng, *Acoustic metamaterials: From local resonances to broad horizons*, Science Advances, 2016.

[4] T. Lee, H. Iizuka, *Bragg scattering based acoustic topological transition controlled by local resonance,* Phys. Rev. B 99, 2019.

[5] S. Babaee, J.T.B. Overelde, E.R.Chen, *Reconfigurable origami-inspired acoustic waveguides,* Science Advances, 2016

[6] H. Yasuda, J. *Yang, Reentrant Origami-Based Metamaterials with Negative Poisson's Ratio and Bistability,* Phys. Rev. Lett. 114, 2015.

[7] H. Yasuda, T. Tachi, M. Lee, J. Yang, *Origami-based tunable truss structures for non-volatile mechanical memory operation*, Nature Communications, 2017

[8] M. Z. Hasan, C. L. Kane, *Colloquium: Topological insulators*, Rev. Mod. Phys, 2010

[9] R. Chaunsali, E. Kim, A. Thakkar, P. G. Kevrekidis, J. Yang, *Demonstrating an In Situ Topological Band Transition in Cylindrical Granular Chains,* Phys. Rev. Lett. 119, 2017

[10] H. Yasuda, Y. Miyazawa, E.G. Charalampidis, C. Chong, P.G. Kevrekidis, J. Yang*, *Origami-based impact mitigation by creating solitary waves with overtaking behavior,* Science Advances (in print, arXiv:1805.05909)

[11] H. Yasuda, J. Yang*, *Tunable frequency band structure of origami-based mechanical metamaterials*, Journal of International Association for Shell and Spatial Structures, 58(4): 287, 2017, invited

[12] Meng Xiao, Z. Q. Zhang, and C. T. Chan, *Surface Impedance and Bulk Band Geometric Phases in One-Dimensional Systems*, Phys. Rev. X 4, 021017, 2014

[13] F. D. M. Haldane and S. Raghu, *Possible Realization of Directional Optical Waveguides in Photonic Crystals with Broken Time-Reversal Symmetry,* Phys. Rev. Lett. 100, 013904, 2008

[14] S. Raghu and F. D. M. Haldane, *Analogs of Quantum-Hall-Effect Edge States in Photonic Crystals*, Phys. Rev. A 78, 033834 (2008).

[15] J. Zak, *Berry's Phase for Energy Bands in Solids*, Phys. Rev. Lett. 62, 2747 (1989).

[16] J. L. du Bois, N. A. J Lieven, S.Adhikari, *Localisation and curve veering: A Different Perspective on Modal Interactions*, Proceeding of the IMAX-XXVII

[17] X. L. Liu, *Behavior of Derivatives of Eigenvalues and Eigenvectors in Curve Veering and Mode Localization and Their Relation to Close Eigenvalues*, Journal of Sound and VibrationVolume 256, Issue 3, 19 September 2002, Pages 551-564

[18] David A. Ehrhardt, Thomas L. Hill, Simon A. Neild, Jonathan E. Cooper, *Veering and nonlinear interactions of a clamped beam in bending and torsion*, Journal of Sound and VibrationVolume 416, 3 March 2018, Pages 1-16

# APPENDIX A